Research Article

14

INDONESIAN SCHOLAR SOCIETY

Indones. J. Chem. Stud.
2026, 5(1), 14–19
Available online at journal.solusiriset.com
e-ISSN: 2830-7658; p-ISSN: 2830-778X

Indonesian Journal of Chemical Studies

Magnetite Functionalized on Graphene Nanoplatelets Surface as Radar Absorbing Matrix in X-Band Region

Krisman Hans Tunggul Purba[1], Andri Hardiansyah[2], M. Zuhnir Pilliang[1], Anisa Salsabila[1], Bintang Dwi Nur Rohmad[3], Riri Murniati[1*]

[1]*Department of Physics, The Republic of Indonesia Defense University, Bogor 16810, Indonesia*

[2]*Research Center for Nanotechnology Systems, National Research and Innovation Agency (BRIN), Banten 15314, Indonesia*

[3]*Department of Chemistry, Brawijaya University, Malang 65145, Indonesia*

Received: 15 Nov 2025; Revised: 27 Jan 2026; Accepted: 27 Jan 2026;
Published online: 31 May 2026; Published regularly: 30 Jun 2026

Abstract— The development of radar absorbing materials (RAM) is a crucial factor in advancing stealth technology, particularly in aerospace and defense sectors. In this study, a nanocomposite consisting of graphene nanoplatelets (GNP) and Ferrous-Ferric Oxide (Fe_3O_4) was successfully synthesized through a mechanical homogenization process using Planetary Ball Milling (PBM). This method was selected to ensure uniform dispersion of the magnetic Fe_3O_4 particles within the conductive GNP matrix, aiming to combine their respective magnetic and dielectric loss mechanisms for enhanced microwave absorption. Surface morphology observations revealed that Fe_3O_4 nanoparticles were homogeneously embedded on the wrinkled surface of the GNP layers, forming a well-integrated nanostructure. X-ray diffraction analysis confirmed that the Fe_3O_4 maintained its characteristic spinel cubic structure following synthesis. The composite exhibited a noticeable reduction in crystallite size and overall crystallinity, which is attributed to the mechanical impact during milling and the disordered nature of GNP. These structural modifications facilitate enhanced multiple scattering and interfacial polarization, which contribute to microwave attenuation. The electromagnetic absorbing performance showed that the GNP/Fe_3O_4 nanocomposite achieved a maximum reflection loss (RL) of –13.9 dB at 11.46 GHz with optimal absorber thicknesses of 3 and 5 mm. Additionally, the composite exhibited a high absorption efficiency of 99.48% (based on through power calculation), indicating excellent performance in the X-band frequency range. Overall, the results suggest that this GNP/Fe_3O_4 nanocomposite offers promising potential as a lightweight, cost-effective, and efficient RAM for stealth technology.

Keywords— *Ferro oxide; Graphene nanoplatelets; Nanocomposites; Planetary ball milling; Radar absorbing material.*

1. INTRODUCTION

In the modern era, advances in military and defence technology continue to drive the need for advanced camouflage systems to avoid radar detection. To achieve this, radar absorbing materials (RAM) are employed. These materials are capable of absorbing electromagnetic waves and converting them into heat energy. Radar detection technology works by using electromagnetic waves (X-band) to identify, locate, and track objects [1]. This field aims to develop RAM materials with excellent radar wave absorption properties. Ideally, RAM must be thin, light, conductive, thermally stable, and corrosion-resistant [2].

Carbon-based materials are utilized in RAM manufacturing due to their unique properties, including being lightweight, having a large surface area, and exhibiting good dielectric properties. One of the carbon-based materials suitable for this application is graphene. Graphene is highly sought after as an electromagnetic wave absorber because of its high dielectric loss and low density [3]. One of the derivative materials of graphene is graphene nanoplatelets (GNP). GNP is a carbon-based nanomaterial with a planar structure consisting of several layers of carbon atoms arranged hexagonally, resulting in a high surface area. GNP has the properties of a large surface area, high electron mobility, high tensile strength, and flexibility [4]. Based on a study by Lee et al [5] graphene monolayer has an elasticity modulus of 1.0 ± 0.1 terapascals (TPa) and an intrinsic tensile strength of 130 ± 10 gigapascals (GPa) at a strain of up to 25%. Zhang et al. [6] successfully synthesized TiO_2/reduced graphene oxide (rGO) via a solvothermal route, which demonstrated a high reflection loss of −42.8 dB at 8.72 GHz. Similarly, Anselmo et al. [7] fabricated GNP/ZnO through planetary ball milling, achieving −28.21 dB at 8.45 GHz. Furthermore, Gita et al. [8] obtained TiO_2/GNP composites using the same

***Corresponding author**.
Email address: ririmurniati90@gmail.com
DOI: 10.55749/ijcs.v5i1.86

milling method, which exhibited a reflection loss of −30.72 dB at 8.42 GHz. These results show that GNPs are promising materials for thermal interface applications and as reinforcement agents in composite structures [9].

In addition to carbon-based materials, materials with strong magnetic properties, such as Ferrous-Ferric Oxide (Fe_3O_4), also exhibit promising magnetic properties. Fe_3O_4 has strong magnetic properties, high permeability, chemical stability, and cost-effectiveness [10], which can enhance RAM performance and is appropriate as a composite material.

Carbon material composite with Fe_3O_4 is a promising option for optimizing RAM performance. According to a study by Liu et al. [11] Graphene@Fe_3O_4@PANI@TiO_2, synthesized via a multi-step method, exhibited a strong ability to absorb electromagnetic waves, achieving a reflection loss of -41.8 dB at 14.4 GHz and a thickness of 1.6 mm. Additionally, the absorption bandwidth corresponding to reflection loss values below −10 dB reached 3.5 GHz. Furthermore, Shang et al. [12] found that a 3D-GNL/Fe_3O_4 composite exhibited a strong attenuation response, reaching a maximum of 46.8 dB over a frequency range of 2-18 GHz.

This study aims to synthesize and evaluate graphene nanoplatelet (GNP)/Fe_3O_4 nanocomposites prepared via the planetary ball milling method for radar-absorbing material (RAM) applications. The technique provides a uniform particle dispersion, enhanced interfacial contact between components, controllable particle size, and improved structural homogeneity. The novelty of this work lies in utilizing GNP within RAM systems, which remains rarely investigated, providing a sustainable pathway for advanced electromagnetic wave absorbers. Structural and morphological characterization were performed using Field Emission Scanning Electron Microscopy with Energy Dispersive X-ray Spectroscopy (FESEM-EDX). Crystal structure analysis was conducted using X-ray Diffraction (XRD). Additionally, to evaluate the electromagnetic wave absorption capability of the materials, the materials' performance was tested using a Vector Network Analyzer (VNA) within the X-band (8–12 GHz) frequency range. The testing was performed by varying the sample thickness from 2 mm to 5 mm to determine the optimal thickness for maximum absorption performance.

2. EXPERIMENTAL SECTION

2.1. Materials & Instrumentations

The materials used in this research were 5.2 g Iron(II) chloride tetrahydrate ($FeCl_3 \cdot 6H_2O$), Iron(III) chloride hexahydrate ($FeCl_2 \cdot 5H_2O$), 5M Sodium hydroxide (NaOH) and Graphene nanoplatelets. All materials were purchased from Sigma-Aldrich and were used without further purification.

Planetary ball mill (RETSCH PM 400, Germany) was utilized to homogenize the nanocomposites. A field emission scanning electron microscope-energy dispersive X-ray (FESEM-EDX, Thermo Scientific Apreo 2 SEM, USA) was used to analyze the nanocomposite's surface structure and elemental composition. X-ray Diffraction (XRD, SMARTLAB RIGAKU, Japan) was utilized to conduct the crystal properties analysis.

The Scherrer equation was used in XRD to calculate the crystallite particle size [13] in **Eq. (1)**. The Scherrer equation utilizes several key variables: k, a shape-related constant (0.9); λ, the X-ray wavelength (0.154 nm); β_{hkl}, which stands for the full width at half maximum (FWHM); and θ_{hkl}, which indicates the peak's position. Additionally, the degree of crystallinity for both Fe_3O_4 and GNP/Fe_3O_4 nanocomposites was assessed to find the ratio, the crystalline peak area (Ac) was divided by the total peak area (Ap), as described in **Eq. (2).** [13, 14].

$$D = \frac{k\lambda}{\beta_{hkl} cos\theta_{hkl}} \quad (1)$$

$$D = \frac{A_c}{A_p} \times 100\% \quad (2)$$

2.2. Synthesis of Fe_3O_4 Nanoparticle

Fe_3O_4 nanoparticles were synthesized by mixing 5.2 g $FeCl_3.6H_2O$ and 2.0 g $FeCl_2.4H_2O$ precursors in 100 mL DI water. The solution was stirred and heated until the temperature reached 60°C. Furthermore, 20 mL of 5 M NaOH was added dropwise until the color of the solution turned black. The temperature was maintained at 60°C, followed by stirring for 5 min. Afterwards, the precipitate was separated using centrifugation for 10 minutes, and then washed with ethanol and deionized (DI) water until the pH was neutral. The precipitate dried in an oven at 60°C for 24 h, and the overall formation of Fe_3O_4 through the coprecipitation mechanism is represented by the reaction **Eq. (3) – (6).**

$$FeCl_3.6H_2O \rightarrow Fe^{3+} + 3Cl^- + 6H_2O \quad (3)$$

$$FeCl_2.4H_2O \rightarrow Fe^{2+} + 2Cl^- + 4H_2O \quad (4)$$

$$Fe^{3+} + 3OH^- \rightarrow Fe(OH)_3 \quad (5)$$

$$Fe^{2+} + 2OH^- \rightarrow Fe(OH)_2 \quad (6)$$

$$Fe(OH)_2 + 2Fe(OH)_3 \rightarrow Fe_3O_4 + 4H_2O \quad (7)$$

2.3. Ball Milling Process of Nanocomposites

The fabrication of Fe_3O_4 /GNP composite was carried out using a planetary ball milling method. Briefly, Fe_3O_4 and GNP were weighed in a mass ratio of 1:1. The powder mixtures were placed into a stainless steel milling vial, followed by the addition of stainless steel balls at a ball-to-powder mass ratio of 2:1. After loading the materials, the vial was securely sealed and placed on a Retsch PM 400 planetary ball mill. The milling process was performed for a total duration of 8 h under ambient conditions.

2.4. Microwave Absorption Performance

The absorption performance of this material is analyzed using a Vector Network Analyzer (VNA) in the

frequency range of 8 to 12 GHz (X-Band), examining sample thicknesses of 2, 3, 4, and 5 mm. The reflection loss (RL) values were calculated from the S11 parameters and validated using the Nicolas-Ross-Weir algorithm [15], which measures the reflection loss (RL) value to assess the material's effectiveness as an electromagnetic wave absorber (RAM). The Reflection Loss (RL) value shows the material's ability to absorb microwaves. The reflection loss (RL) profiles of GNP/Fe_3O_4 were obtained based on the permittivity and permeability at specific frequencies and sample thicknesses, as described by the transmission line theory. The relationship is represented in **Eq. (8)** and **Eq. (9)** [16, 17].

$$Z_{in} = Z_0(\mu_r/\varepsilon_r)^{1/2}\tanh[j(\tfrac{2\pi fd}{c})(\mu_r\varepsilon_r)^{1/2}] \quad (8)$$

$$RL = 20\log|(Z_{in} - Z_0)/(Z_{in} + Z_0)| \quad (9)$$

In these equations, Z_{in} represents the input impedance of the absorber, Z_0 is the impedance of free space, μ_r is the relative complex permeability, εr is the complex permittivity, f is the microwave frequency, d is the thickness of the absorber, and c is the speed of light in vacuum. An RL value of -10 dB indicates that approximately 90% of microwave energy is absorbed. Generally, materials with RL values of less than –10 dB are considered suitable for absorbing EM waves [18]. Reflection loss (RL) values can be used to find the value of the absorption coefficient or trough power using **Eq. (10)** and **Eq. (11)**.

$$|\tau| = 10^{RL/20} \quad (10)$$

$$Through\ power\ (\%) = (1 - \tau) \times 100\% \quad (11)$$

3. RESULT AND DISCUSSION

3.1. Mechanism Fe_3O_4 & GNP/Fe_3O_4

The formation mechanism of Fe_3O_4 and GNP/Fe_3O_4 nanocomposites is described together to provide a more precise and continuous explanation, as suggested by the reviewer. The Fe_3O_4 nanoparticles were synthesized via the co-precipitation method, where $FeCl_3{\cdot}6H_2O$ and $FeCl_2{\cdot}4H_2O$ with a mass proportion of 5.2:2 were dissolved in 100 mL of deionized water to produce Fe^{3+} and Fe^{2+} ions. The dropwise addition of 20 mL NaOH solution (3 M) under constant stirring initiated the formation of $Fe(OH)_3$ and $Fe(OH)_2$ intermediates, which subsequently underwent dehydration and electron transfer to form Fe_3O_4 nanoparticles. Particle growth proceeded through Ostwald ripening, yielding well-dispersed Fe_3O_4 [19].

To develop the GNP/Fe_3O_4 nanocomposites, the Fe_3O_4 nanoparticles were combined with GNP using planetary ball milling. The repeated high-energy collisions during milling reduced the particle size of Fe_3O_4 and exfoliated the GNP layers, generating thinner graphene sheets. This process also promoted strong physical interaction between Fe_3O_4 and GNP through mechanical interlocking, supported by continuous impact and mixing [20]. A visual illustration of the complete formation process of GNP/Fe_3O_4 nanocomposites is presented in **Fig. 1.**

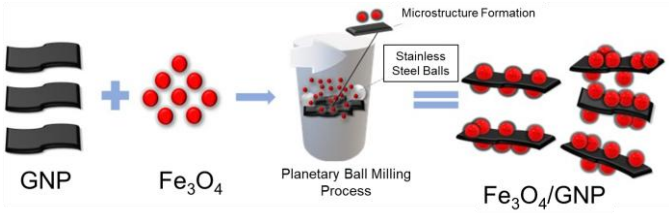

Fig. 1 Formation mechanism of GNP/Fe_3O_4 nanocomposites via planetary ball milling

3.2. Structure and Morphology Analysis

Fig. 2(a) presents the morphology of the Fe_3O_4/GNP composite, which exhibits irregular spherical agglomerates with particle sizes ranging from approximately 50 to 150 nm. The Fe_3O_4/GNP particles undergo size reduction during the high-energy ball milling process. The graphene nanoplatelets (GNP), a carbon-based material composed of thin, sheet-like structures, undergo fragmentation or folding during milling, thereby integrating into a matrix with Fe_3O_4 particles. This structure may trigger a polarization interference [21]. The high mechanical energy generated during milling promotes intimate contact between Fe_3O_4 and GNP components, leading to strong interfacial interactions.

The elemental mapping analysis via EDX confirms both the composition and spatial distribution of elements within the composite. **Fig. 2(b)** shows the distribution of carbon (C), which is uniformly and extensively spread throughout the sample area, affirming the presence of GNP as a primary matrix component. The EDS mapping indicates that the significant elements in the Fe_3O_4/GNP composite are carbon (C), oxygen (O), and iron (Fe). The strongest peak corresponds to carbon, reflecting the dominant contribution of graphene nanoplatelets (GNP) to the overall composition, followed by distinct peaks of oxygen and iron that confirm the successful incorporation of Fe_3O_4 into the composite matrix.

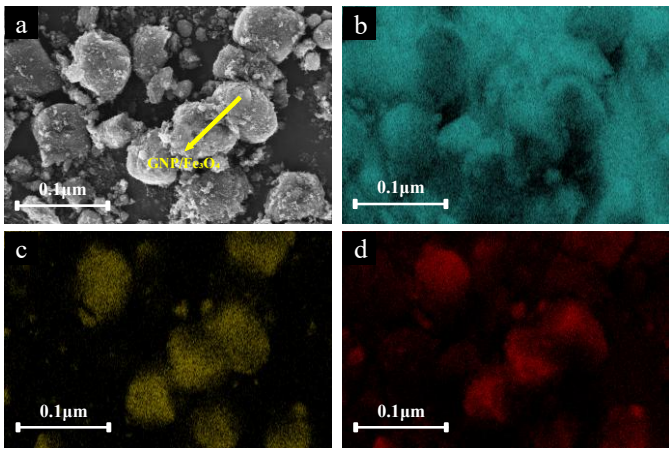

Fig. 2 (a) FESEM-EDX analysis of FESEM GNP/Fe_3O_4 nanocomposites, and EDX mapping of (b) Carbon, (c) Iron, and (d) Oxygen atoms.

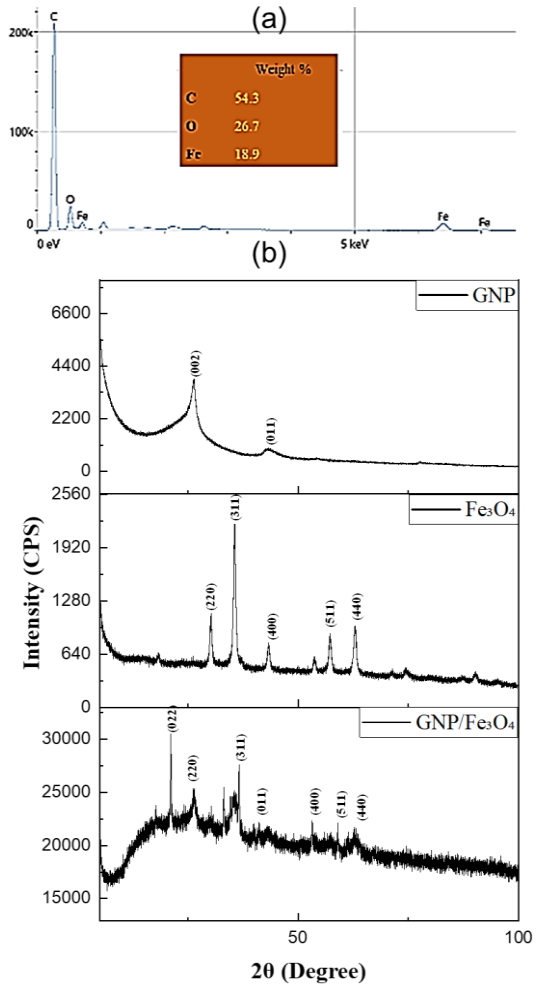

Fig. 3 (a) Map sum mapping of GNP/Fe_3O_4 nanocomposites, (b) XRD diffractogram of GNP, Fe_3O_4, and GNP/Fe_3O_4 nanocomposites

Meanwhile, **Fig. 2(c)** and **Fig. 2(d)** represent the distribution of iron (Fe) and oxygen (O), respectively, which are clearly localized in the same regions as the particles observed in the FESEM image, confirming the existence of Fe_3O_4. The strong spatial correlation between Fe and O indicates the stable formation of Fe_3O_4, and the overlapping distribution of all three elements (C, Fe, and O) provides compelling evidence that the planetary ball milling method successfully produced the Fe_3O_4/GNP composite. The relatively homogeneous dispersion of Fe_3O_4 particles within the GNP matrix, as revealed by the elemental maps, indicates effective mixing and strong interaction between the two components at the nanoscale. According to the map sum mapping in **Fig. 3(a)**, the GNP/Fe_3O_4 nanocomposites are composed of 54.3% carbon, 26.7% oxygen, and 18.9% iron.

The X-ray diffractograms of all synthesized materials were evaluated in the 2θ range of 20–90°, as shown in **Fig. 3(b)**. The XRD pattern of GNP exhibited two primary diffraction peaks at 2θ = 29.41° and 42.19°, corresponding to the (022) and (011) planes, respectively. These peaks are characteristic of the layered hexagonal carbon structure, confirming the presence of stacked graphene sheets. Based on the Scherrer calculation, the crystallite sizes of GNP were approximately 8.21 nm for the (022) plane and 8.52 nm for the (011) plane, indicating the formation of nanoscale graphitic domains. Although the peak intensity of GNP was relatively broad, the purity of the graphene phase was verified from the absence of impurity-related peaks.

The X-ray diffractogram of Fe_3O_4 displays several sharp and high-intensity peaks at 30.29°, 35.65°, 43.29°, 57.25°, and 62.87°, which correspond to the (220), (311), (400), (511), and (440) crystal planes. These peaks match the standard magnetite phase with an inverse spinel cubic structure. The crystallite sizes calculated using the Scherrer equation were 32.92 nm, 33.38 nm, 34.19 nm, 36.20 nm, and 37.24 nm for each respective plane, confirming the formation of well-crystallized magnetite nanoparticles.

The X-ray diffractograms of the GNP/Fe_3O_4 nanocomposite showed clearly combines the distinct characteristic peaks of both GNP and Fe_3O_4, indicating the successful formation of the hybrid nanostructure. The composite exhibits diffraction peaks at the same 2θ positions as its constituent materials—Fe_3O_4 peaks at 30.29°, 35.65°, 43.29°, 57.25°, and 62.87°, and GNP peaks at 29.41° and 42.19°. The crystallite sizes of the GNP/Fe_3O_4 nanocomposite were calculated to be in the range of 23.47–26.60 nm, reflecting the combined effect of particle refinement and structural disorder from the ball milling process.

3.3. Microwaves Absorbing Performance

Fig. 4 shows the VNA results of GNP/Fe_3O_4 nanocomposites with thickness variations of 2, 3, 4, and 5 mm. At a thickness of 2 mm, the composite exhibited a main absorption peak at 11.45 GHz with an RL of –12.1 dB and a through power of 99.3%, indicating effective absorption within the X-band frequency range. Increasing the thickness to 3 mm resulted in a deeper RL of –13.9 dB at 11.46 GHz, with a through power of 99.4%. The 4 mm sample showed an RL of –13.8 dB at

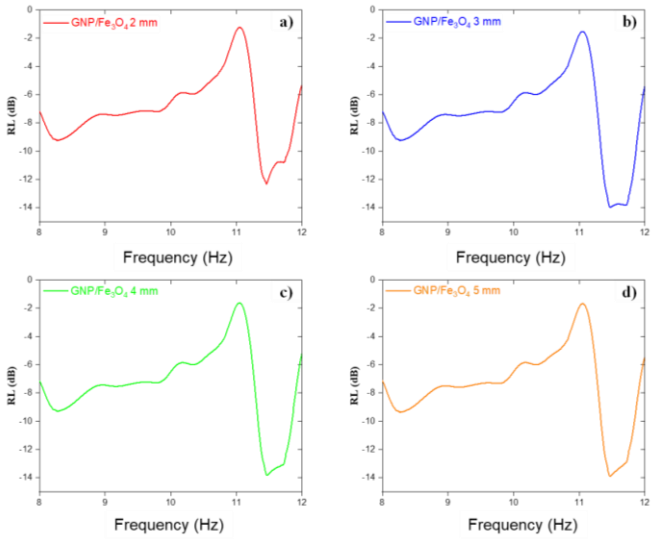

Fig. 4 VNA results of GNP/Fe_3O_4 nanocomposites at 2–5 mm thickness.

the same frequency, while the 5 mm sample again achieved an RL of –13.9 dB at 11.46 GHz, demonstrating stable absorption performance even at increased thickness. As illustrated in Table 1, all GNP/Fe_3O_4 samples consistently exhibited low RL values and high through-power attenuation across the thickness range of 2–5 mm (**Table 1**).

A detailed analysis shows that all tested thicknesses achieved RL values of –10 dB or lower, corresponding to over 90% microwave attenuation [22], confirming the excellent performance of GNP/Fe_3O_4 as a RAM. The observed enhancement in absorption with increased thickness is attributed to improved impedance matching and a lower attenuation constant, which becomes more favorable due to the extended path length for electromagnetic wave propagation within the material [23]. This is further supported by the observation that the 3 mm and 5 mm samples exhibit identical peak RL values (–13.9 dB). Such behavior is commonly attributed to multiple thicknesses satisfying similar quarter-wavelength (λ/4) matching conditions, where increasing thickness beyond the optimal point does not significantly alter the destructive interference mechanism responsible for strong absorption.

The synergistic effect between dielectric and magnetic losses in GNP/Fe_3O_4 nanocomposites enables strong absorption even at relatively thin profiles, making them highly suitable for practical electromagnetic interference (EMI) shielding and stealth applications.

Table 1. RL and through power of GNP/Fe_3O_4 nanocomposites at 2 to 5 mm thickness

Thickness (mm)	Frequency (Hz)	RL Value (dB)	Through Power (%)
2	11.45	-12.1	99.33
3	11.46	-13.9	99.48
4	11.46	-13.8	99.47
5	11.46	-13.9	99.48

4. CONCLUSION

The GNP/Fe_3O_4 nanocomposite was effectively synthesized through a mechanical homogenization method using Planetary Ball Milling. Structural and morphological evaluations using XRD and FE-SEM confirmed the formation of a GNP matrix with uniformly dispersed Fe_3O_4 particles, accompanied by a reduction in crystallite size, which supports enhanced microwave attenuation. These structural characteristics contribute to the composite's ability to efficiently absorb electromagnetic waves. The GNP/Fe_3O_4 nanocomposite exhibited a maximum absorption performance, with a reflection loss of –13.9 dB at 11.46 GHz and an absorption rate of 99.48% at both 3 mm and 5 mm thicknesses. This study highlights the material potential of lightweight and efficient candidates for radar absorbing materials (RAM). This nanocomposite, comprising conductive and magnetic components, provides a practical solution for stealth technology and the mitigation of electromagnetic interference (EMI).

5. AUTHOR'S DECLARATION

5.1. Supporting Information

This manuscript does not include supplementary supporting information. However, all data underlying the findings of this study are available from the corresponding author (RM) upon reasonable request.

5.2. Acknowledgements

We gratefully acknowledge the support provided by the Nanocarbon Functional Research Group, National Research and Innovation Agency (BRIN).

5.3. Conflict of Interest

There was no conflict of interest in this study.

5.4. Author Contributions

KHTP, AH, AS, BDNR, RM, and MZP contributed equally to this research. The study was jointly designed and carried out by all listed authors, who also supervised the characterization process. RM and MZP contributed to revising the manuscript. All authors have reviewed and approved the final version of this manuscript.

5.5. AI Statement

ChatGPT was utilize to enhance the clarity, grammar, and overall readability of this manuscript. All technical content, data interpretation, and conclusion were solely developed and verified by the authors. The final version of the manuscript was thoroughly reviewed to ensure accuracy, coherence, and aligment with the study's findings.

6. REFERENCES

[1] Yang, J., Pang, Y., Cai, G., Zheng, H., Wang, J., Li, Y. and Xu, Z. 2025. Design, modelling, and validation of electrically tunable multifunctional composites with dynamic control properties from transmission to absorption. *Compos. Part A Appl. Sci. Manuf.* 199. 109261. doi: https://doi.org/10.1016/j.compositesa.2025.109261

[2] Ruiz-Perez, F., López-Estrada, S.M., Tolentino-Hernández, R.V. and Caballero-Briones, F. 2022. Carbon-based radar absorbing materials: A critical review. *J. Sci.: Adv. Mater. Devices*. 7(3). 100454. doi: https://doi.org/10.1016/j.jsamd.2022.100454

[3] Sun, X., He, J., Li, G., Tang, J., Wang, T., Guo, Y. and Xue, H. 2013. Laminated magnetic graphene with enhanced electromagnetic wave absorption properties. *J. Mater. Chem. C.* 1(4). 765-777. doi: https://doi.org/10.1039/C2TC00159D

[4] A Nag, A., Alahi, M.E.E. and Mukhopadhyay, S.C. 2021. Recent progress in the fabrication of graphene fibers and their composites for applications of monitoring human activities. *Appl Mater. Today*. 22. 100953. doi: https://doi.org/10.1016/j.apmt.2021.100953

[5] Lee, C., Wei, X., Kysar, J.W. and Hone, J. 2008. Measurement of the elastic properties and intrinsic strength of monolayer graphene. *Science*. 321(5887). 385-388. doi: https://doi.org/10.1126/science.1157996.

[6] Zhang, H., Zhao, Y., Yang, X., Zhao, G., Zhang, D., Huang, H., Yang, S., Wen, N., Javid, M., Fan, Z. and Pan, L. 2020. A facile synthesis of novel amorphous TiO_2 nanorods decorated rGO hybrid composites with wide band microwave absorption. *Nanomaterials*. 10(11). 2141. doi:

https://doi.org/10.3390/nano10112141

[7] Rasendriya, A.B., Hardiansyah, A., Amalia, G.R., Rahmadtullah, I., Setiono, A., Piliang, M.Z. and Renta, H. 2025. Fabrication and characterization of graphene nanoplatelets/zinc oxide nanocomposites as a military radar absorbing material. *Indones. J. Chem. Stud*. 4(1). 28-34. doi: https://doi.org/10.55749/ijcs.v4i1.69

[8] Amalia, G.R., Hardiansyah, A., Rasendriya, A.B., Rahmadtullah, I., Setiono, A., & Murniati, R. 2025. Synthesis and characterization of titanium dioxide/graphene nanoplatelets nanocomposites via planetary ball milling for military radar absorbing materials. *Indones. J. Chem. Stud.* 4(1). 22–27. doi: https://doi.org/10.55749/ijcs.v4i1.67

[9] Cataldi, P., Athanassiou, A. and Bayer, I.S. 2018. Graphene nanoplatelets-based advanced materials and recent progress in sustainable applications. *Appl. Sci.* 8(9). 1438. doi: https://doi.org/10.3390/app8091438

[10] Yavuz, C.T., Mayo, J.T., Yu, W.W., Prakash, A., Falkner, J.C., Yean, S., Cong, L., Shipley, H.J., Kan, A., Tomson, M. and Natelson, D. 2006. Low-field magnetic separation of monodisperse Fe_3O_4 nanocrystals. *Science*. 314(5801). 964-967. doi: https://doi.org/10.1126/science.1131475

[11] Liu, P., Huang, Y., Yang, Y., Yan, J. and Zhang, X. 2016. Sandwich structures of graphene@ Fe_3O_4@ PANI decorated with TiO_2 nanosheets for enhanced electromagnetic wave absorption properties. *J. Alloys Compd.* 662. 63-68. doi: https://doi.org/10.1016/j.jallcom.2015.12.022

[12] Shang, T., Lu, Q., Zhao, J., Chao, L., Qin, Y., Ren, N., Yun, Y. and Yun, G. 2021. Novel three-dimensional graphene-like networks loaded with Fe_3O_4 nanoparticles for efficient microwave absorption. *Nanomaterials.* 11(6). 1444. doi: https://doi.org/10.3390/nano11061444

[13] Nasiri, S., Rabiei, M., Palevicius, A., Janusas, G., Vilkauskas, A., Nutalapati, V. and Monshi, A. 2023. Modified Scherrer equation to calculate crystal size by XRD with high accuracy, examples Fe_2O_3, TiO_2 and V_2O_5. *Nano Trends*. 3. 100015. doi: https://doi.org/10.1016/j.nwnano.2023.100015

[14] Uzun, İ. 2023. Methods of determining the degree of crystallinity of polymers with X-ray diffraction: a review. *J. Polym. Res.* 30(10). 394. doi: https://doi.org/10.1007/S10965-023-03744-0

[15] Negi, P. and Kumar, A. 2022. Biomass-Derived activated carbon/epoxy composite as microwsave absorbing material. *J. Electron. Mater.* 51(6). 2918-2925. doi: https://doi.org/10.1007/s11664-022-09558-y/tables/2

[16] Mashadi, M., Suyanti, S., Setiawan, J., Yunasfi, Y. and Adi, W.A. 2023. Magnetic and microwave absorbing properties of cerium substituted zinc ferrite synthesized using milling technique. *J. Supercond. Nov. Magn.* 36(2). 721-731. doi: https://doi.org/10.1007/s10948-023-06518-3

[17] Mu, Y., Ma, Z.H., Liang, H.S., Zhang, L.M. and Wu, H.J. 2022. Ferrite-based composites and morphology-controlled absorbers. *Rare Met.* 41(9). 2943-2970. doi: https://doi.org/10.1007/s12598-022-02045-7

[18] Huo, Y., Tan, Y., Zhang, F., Cui, W., Wang, Y. and He, Z. 2024. Binary nickel ferrite/carbon hybrid nanofibers for multiband, strong electromagnetic wave absorption. *J. Alloys Compd.* 993. 174676. doi: https://doi.org/10.1016/j.jallcom.2024.174676

[19] Elamin, N.Y., Modwi, A., Abd El-Fattah, W. and Rajeh, A. 2023. Synthesis and structural of Fe_3O_4 magnetic nanoparticles and its effect on the structural optical, and magnetic properties of novel Poly (methyl methacrylate)/Polyaniline composite for electromagnetic and optical applications. *Opt. Mater.* 135. 113323. doi: https://doi.org/10.1016/j.optmat.2022.113323

[20] Cui, X., Gong, P., Wang, C., Zhang, Y., Zhang, W., Zhang, Z., Zhou, Z., Chen, X., Feng, Y., Xu, L. and Xin, H. 2025. Enhanced lubrication mechanism and performance of Fe_3O_4/graphene nanolubricant under magnetic field. *Chin. J. Mech. Eng.* 39. 100034. doi: https://doi.org/10.1016/J.cjme.2025.100034

[21] Setua, D.K., Mordina, B., Srivastava, A.K., Roy, D. and Prasad, N.E. 2020. Carbon nanofibers-reinforced polymer nanocomposites as efficient microwave absorber. In *Fiber-reinforced nanocomposites: fundamentals and applications*. 395-430. doi: https://doi.org/10.1016/B978-0-12-819904-6.00018-9

[22] Liu, P., Gao, S., Wang, Y., Huang, Y., Wang, Y. and Luo, J. 2019. Core–shell CoNi@ graphitic carbon decorated on B, N-codoped hollow carbon polyhedrons toward lightweight and high-efficiency microwave attenuation. *ACS Appl. Mater. Interfaces.* 11(28). 25624-25635. doi: https://doi.org/10.1021/acsami.9b08525

[23] Zhong, Y., Long, Y., Sun, Y., Qin, J., Li, Y., Liang, G., Zou, J. and Xie, P., 2025. Ultra-lightweight carbon nanocomposites as microwave absorber with high absorbing performance derived from flour. *Adv. Compos. Hybrid Mater.* 8(1). 21. doi: https://doi.org/10.1007/S42114-024-01080-5